Ice Nucleation and Phase Behavior on Oligo(ethylene glycol) and Hydroxyl Self-Assembled Monolayers: Simulations and Experiments

Mattias Östblom,[†] Ramunas Valiokas,[†] Peter Konradsson,[‡] Stefan C. T. Svensson,[‡] and Bo Liedberg*,[†]

Divisions of Molecular Physics and Organic Chemistry, Department of Physics, Chemistry and Biology, Linköping University, SE-581 83 Linköping, Sweden

Matthew Garrett and David L. Allara

Department of Chemistry and Materials Science, Pennsylvania State University, University Park, Pennsylvania 16802

Received: October 20, 2005; In Final Form: December 1, 2005

The nucleation and phase behavior of ultrathin D_2O-ice overlayers have been studied on oligo(ethylene glycol) (OEG)-terminated and hydroxyl self-assembled monolayers (SAMs) at low temperatures in ultrahigh vacuum. Infrared reflection−absorption spectroscopy (IRAS) is used to characterize the ice overlayers, the SAMs, and the interactions occurring between the ice and the SAM surfaces. Spectral simulations, based on optical models in conjunction with Maxwell Garnett effective medium theory, point out the importance of including voids in the modeling of the ice structures, with void fractions reaching 60% in some overlayers. The kinetics of the phase transition from amorphous-like to crystalline-like ice upon isothermal annealing at 140 K is found to depend on the conformational state of the supporting OEG SAM surface. The rate is fast on the helical OEG SAMs and slow on the corresponding all-trans SAMs. This difference in kinetics is most likely due to a pronounced D_2O interpenetration and binding to the all-trans segments of the ethylene glycol portion of the SAM. No such penetration and binding was observed on the helical OEG SAM.

Introduction

Organothiolate self-assembled monolayers (SAMs) on gold[1] with variable terminal functionality have become of increasing interest in the past two decades for applications extending into areas such as biosensing,[2−6] electrochemistry,[7−10] tribology,[11,12] and supported biological membranes.[4,13−15] The protein adsorption characteristics onto SAMs also have been explored for biomedical applications and several investigations aiming at producing a surface that resists protein adsorption have been reported.[16−18] In particular, OEG-grafted surfaces display very promising protein rejecting properties and the importance of the OEG chain length, mobility, and conformation has been thoroughly discussed.[19−24] It is also becoming increasingly clear that interfacial water plays a crucial role for molecular interactions occurring at or near mineral, organic, and biological materials/surfaces.[25−27] Thus, studies of the role of interfacial water on protein−surface interaction and deposition seem to be a highly relevant and justified topic for the development of new and improved biomaterials. Water at or close to organic surfaces may, for example, display different physiochemical properties as compared to bulk water, and these issues have been addressed by Grunze and co-workers in a series of theoretical and experimental reports with OEG SAMs as the model system.[28−32] We also have previously studied the properties of interfacial water in the form of ultrathin ice overlayers on organic SAMs.[33−37] The vast majority of these investigations have been devoted to studies of the phase behavior of ice on SAMs with well-defined wettability properties. Morphological changes of the ice overlayer upon thermal annealing have also been studied.[34] The aim of the present work is to increase the understanding of nucleation and phase behavior of ultrathin ice on SAMs bearing relatively complex terminal groups. The dynamic structure (phase behavior) of the ice overlayer, ∼2 monolayers (ML) thick, as well as the interaction(s) with the SAM surface groups are examined with infrared reflection−absorption spectroscopy (IRAS) before, during, and after isothermal annealing in ultrahigh vacuum (UHV) utilizing SAMs of *ω*-substituted *n*-alkanethiols bearing oligo(ethylene glycol) tail groups of different lengths, Scheme 1. The tail groups investigated are hexa(ethylene glycol) (EG_6) and di(ethylene glycol) (EG_2), which are known to assemble in two different conformations on gold. The EG_6 compound assembles predominantly in a helical conformation with a small fraction of amorphous and all-trans conformers, whereas EG_2 assembles in the all-trans conformation.[19] The behavior of ice on a hydroxyl-terminated, hydrophilic SAM is also examined for comparison.

SCHEME 1: Molecules Used for Creating Self-Assembled Monolayers

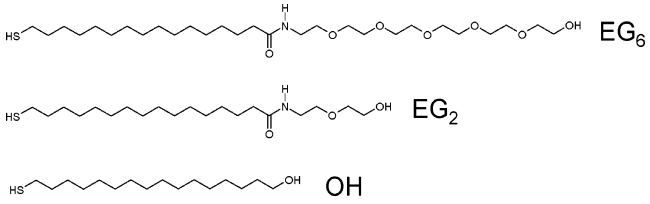

* Address correspondence to this author. E-mail: bolie@ifm.liu.se. Phone: +46-13-281877. Fax: +46-13-288969.
[†] Division of Molecular Physics, Linköping University.
[‡] Division of Organic Chemistry, Linköping University.

10.1021/jp056007q CCC: $33.50
Published on Web 01/10/2006

Extensive spectral simulations of the ice overlayer structure and phase behavior are also undertaken to support the interpretation of the experimental reflection absorption (RA) spectra. Most importantly, our simulations show that excellent agreement with experimental data can be obtained by introducing voids in the modeling of the ice overlayer structures. This is an extension as compared to our previous work[37] where the simulations of the ice structure were based exclusively on bulk optical data of hexagonal (Ih) and amorphous (Ia), D_2O-ice. Moreover, the present IRAS experiments clearly show that the kinetics of the phase transition from amorphous to crystalline ice, upon isothermal annealing, depends on the conformation of the OEG portion. The slow kinetics observed on the all-trans OEG-SAMs is discussed in terms of a reduced surface mobility caused by partial interpenetration of the D_2O molecules into the all-trans assembly.

Experimental Section

Sample Preparation and Infrared Analysis. The synthesis of the oligo(ethylene glycol) thiols EG_2 and EG_6, Scheme 1, has been described elsewhere.[38] 16-Mercaptohexadecanol (OH) was obtained as a generous gift from Dr. Stefan Löfås, Biacore Intl., Uppsala, Sweden.

The substrates used for self-assembly were prepared by electron-beam evaporation of 2000 Å thick gold on top of freshly cleaned (100) silicon substrates primed with a 25 Å thick adhesive layer of titanium. All evaporations took place in a Balzers UMS 500 P system operating at a base pressure on the low 10^{-9} Torr scale and an evaporation pressure on the low 10^{-7} Torr scale. The evaporation rate was 10 Å/s for gold and 1 Å/s for titanium. The samples were thoroughly cleaned in a 5:1:1 mixture of distilled water:25% hydrogen peroxide:30% ammonia for 10 min at 80 °C prior to incubation in the thiol solutions. The samples were incubated for a minimum of 15 h in a 20 μM ethanol solution (99.5%, Kemetyl, Stockholm, Sweden) of the desired thiol. After incubation the samples were rinsed with ethanol, ultrasonicated in ethanol for 3 min to remove thiols not covalently attached to the gold surface, rinsed in ethanol again, and finally blown dry in N_2. The samples were immediately inserted in the UHV system to reduce the exposure to airborne species, and the measurement of the sample began 2 h after insertion. All samples were investigated at room temperature with IRAS to confirm the structure of the deposited monolayer. The sample was subsequently cooled to 85 K via a liquid nitrogen Cu finger, and another RA spectrum was recorded to identify the changes in the SAM conformation with temperature. This 85 K spectrum also served as a reference spectrum during calculation of the RA spectrum of the ice−SAM interaction. D_2O (Merck) was deposited onto the SAM via a capillary tube in front of the sample stage. The amount of deposited D_2O onto the sample surface was repeatable within 10%, and the rate of deposition was 0.2 ML/s (0.6 Å/s). Another RA spectrum was recorded immediately after deposition of the D_2O-ice overlayer on the SAM surface. The 85 K spectrum was subtracted from the D_2O-ice (85 K) spectrum to reveal the effect of the deposited D_2O-ice overlayer on the SAM conformation, and to investigate the structural properties and phase behavior of the deposited D_2O-ice overlayer. The D_2O-ice overlayers were subsequently annealed at 140 K for 60 min, and the D_2O-ice structure was continuously studied with IRAS. This annealing temperature was chosen to ensure a very low desorption rate of D_2O-ice from the SAM surface. The UHV system used to prepare and analyze the D_2O-ice overlayer has been described in detail elsewhere.[36] All RA spectra reported herein were recorded at a spectral resolution of 2 cm^{-1}.

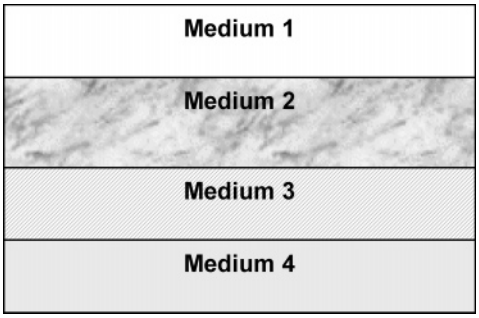

Figure 1. Model of the sample used in the simulation of the RA spectra. Medium 1: Air ($n = 1.00$, $k = 0.00$), infinite thickness. Medium 2: D_2O-ice; ice Ia, ice Ih, and/or void, variable thickness depending on the amount of void. Medium 3: SAM ($n = 1.45$, $k = 0.00$), thickness depends on SAM. Medium 4: Gold layer, variable n, k, infinite thickness. A thickness of 2000 Å can be regarded as infinitely thick for a metal like gold in the mid-infrared region. The angle of incidence for the simulations is 83° with respect to the surface normal and for light polarized parallel to the plane of incidence.

Spectral Simulations. Simulations of the experimental RA spectra of D_2O-ice are based on calculations of classical electromagnetic field interactions with a sample modeled as a stack of planar, parallel layers (Figure 1), each described in terms of thickness and a uniform, isotropic complex optical (or dielectric) response function spectrum $\hat{n}_j(\tilde{\nu}) = n_j(\tilde{\nu}) + ik_j(\tilde{\nu})$, where j = the jth layer, $\tilde{\nu}$= frequency (wavenumbers), and $n_j(\tilde{\nu})$ and $k_j(\tilde{\nu})$ are the real (refractive index) and imaginary (extinction) parts of the optical function, respectively. Once the layer thicknesses, optical response functions, and IR beam characteristics (angle of incidence and E-field polarization) are assigned numerical values, algorithms based on the standard electromagnetic theory of wave propagation through layered media are applied to calculate spectra which then can be compared with the experimental spectra.[39,40] Through an iteration process the model parameters can be varied until a best fit with experiment is reached. The parameters used in the modeling are displayed in the legend of Figure 1. Optical constants for gold are taken from Palik,[41] and optical constants for Ia-ice and Ih-ice are from Bergren et al.[42]

A previous report utilized this approach to model RA spectra of D_2O-ice overlayers.[37] However, in the present approach we now have also allowed for different volume fractions of the two ice phases, with or without voids, to be present in the ice overlayer. The Maxwell Garnett effective medium approximation,[43,44] eq 1, was used to obtain the effective dielectric function of the ice overlayer,

$$\epsilon_{MG}(\nu) = \epsilon_1 \frac{\epsilon_2 + 2\epsilon_1 + 2f_2(\epsilon_2 - \epsilon_1)}{\epsilon_2 + 2\epsilon_1 - f_2(\epsilon_2 - \epsilon_1)} \qquad (1)$$

where $\epsilon_{MG}(\nu)$ represents the effective Maxwell Garnett dielectric function. ϵ_1 and ϵ_2 are the dielectric constants for the fractions of higher and lower composition, respectively, and f_2 is the volume fraction of the lower composition. This approach has been successful in the past for modeling the RA spectra of heterogeneous molecular films caused by dewetting of SAMs.[45,46] The Maxwell Garnett approach is particularly useful when the two phases in the modeled layer display a large optical contrast, e.g., as in the case of mixing voids (air) and Ih-ice. Since it was not possible for us to measure directly the thickness of a composite void ice overlayer it was necessary to make an indirect determination. In our previous work[37] we developed a method to estimate the overlayer thickness of amorphous ice, the dominant phase formed on SAMs, at low temperature (e.g.,

85 K). This thickness was used as a starting point to simulate a number of RA spectra for a range of nearby thicknesses, and the thickness that gives the best fit to the experimental RA spectrum was selected from that range. For ice overlayers containing varying amounts of voids, an inherent assumption was made for all simulations stating that the mass of ice on the surface remained the same at all times (conservation of mass). This assumption is reasonable considering the negligible rate of desorption during isothermal annealing at 140 K. The thickness of the layer is in this particular case proportional to the amount of voids present in the layer. Thus, the only varying parameters are the relative proportions of amorphous and polycrystalline ice, the relative amount of voids, and the resulting thickness due to void insertion. In these analyses, it is also possible to consider applying the Bruggeman Effective Medium Approximation rather than the Maxwell Garnett Approximation. We find, however, that for our samples the two sets of results are nearly identical. Details of the comparison are presented in the Supporting Information.

Results and Discussion

Simulations of RA Spectra of D_2O-Ice. An experiment is first shown to demonstrate the significance of considering voids in the ice films. A sample was obtained by depositing a thick layer ~30 Å of D_2O-ice on a 16-mercaptohexadecanol (OH) SAM surface at 85 K. This ice layer was then annealed at 150 K for 20 min to reach a final thickness of ~6 Å (the desorption rate is significant at 150 K), equivalent to ~2 ML, and to ensure that the remaining ice layer adopts a crystalline-like conformation. In earlier work, while we showed that RA spectra of Ia D_2O-ice layers deposited at 120 K on SAMs can be simulated accurately,[37] particularly for high energy surfaces, with the ice layers existing at the normal bulk phase density, it also was observed that the simulations showed consistently poor fits over a wide range of parameter space for films containing crystalline-like, Ih-ice. This problem is also illustrated in Figure 2a, which shows the experimental RA spectrum of the annealed, ~2 ML (~6 Å) thick residual D_2O-ice layer on the hydroxyl SAM, along with a series of simulations using optical constants of bulk density ice.[42] It is evident that simulated RA spectra for various Ih/Ia mixtures poorly reproduce the experimental data. This discrepancy can be accounted for by including voids in the Ih phase. Figure 2b shows a set of simulated RA spectra where voids have been introduced in various proportions (0−60%) into a pure Ia (bottom set of spectra) and a pure Ih phase overlayer (top set of spectra). Simulations were performed after including various amounts of voids in the model to obtain the Maxwell Garnett effective dielectric functions, $\epsilon_{MG}(\nu)$. Note that while the introduction of voids in both Ia- and Ih-ice overlayers increases the overall intensity of the main peak and shifts the peaks toward lower frequencies, a comparison with the experimental spectrum (middle panel) reveals that the simulated peaks only start to match experiment for the case of void insertion in the pure Ih phase, with an excellent fit at a void content of 60%, as seen in Figure 2c. From this simulation we conclude that the overlayer in this ~2 ML sample is essentially ~60% porous Ih-ice. It should be stressed, however, that the Maxwell Garnett effective medium approximation is only considered useful for void fractions up to about 60%. A comprehensive discussion about the applicability of the Maxwell Garnett theory as well as other effective medium theories can be found in the literature[47−49] and partly in the Supporting Information.

Ultrathin D_2O layers were also prepared on OEG SAMs, and the Maxwell Garnett approach, in combination with spectral simulations, was again employed to assist in the interpretation of the experimental data. Figure 3 shows RA spectra for "as deposited" D_2O-ice overlayers (~2 ML) on EG_2 and EG_6 SAMs (see Scheme 1), respectively, at 85 K. The sample temperature for the "as deposited" D_2O-ice overlayer was then raised to 140

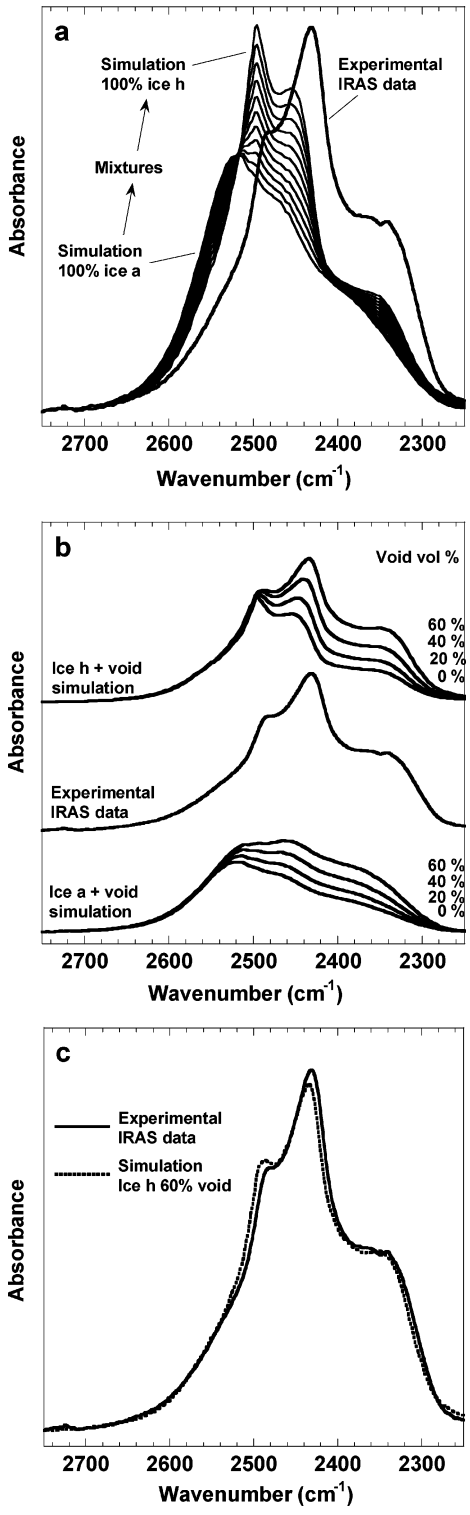

Figure 2. Simulated and experimental RA spectra for ~2 ML of D_2O-ice on a hexadecanol thiol (OH) SAM surface. (a) Simulated RA spectra for different mixtures of Ih and Ia D_2O-ice. Also shown is the experimental RA spectrum. (b) Top panel: Simulated RA spectra of Ih-ice with different void fractions (0−60%). Middle panel: Experimental RA spectrum. Lower panel: Simulated RA spectra of Ia-ice with different volume fractions void. (c) Comparison between the experimental RA spectrum and the best fit, using Ih-ice with 60% void.

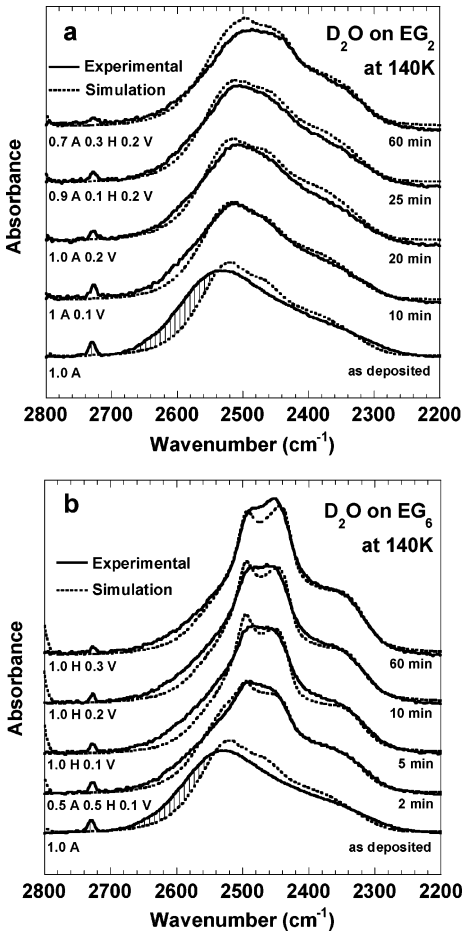

Figure 3. Evolution of RA spectra of D_2O-ice upon isothermal annealing at 140 K for different periods of time (solid lines). The RA spectrum at the bottom is obtained for an "as deposited" D_2O-ice layer at 85 K. Also shown are the best fits (dotted lines). (a) RA spectra for ~2 ML of D_2O-ice on an EG_2 SAM (all-trans). (b) RA spectra for ~2 ML of D_2O-ice on an EG_6 SAM (helical).

K at a rate of approximately 1 deg/min before it was subjected to isothermal annealing at 140 K for 60 min. The structural changes occurring within the D_2O-ice overlayers as well as the interaction(s) with the SAM surface (more about that later) were continuously monitored. The experimental RA spectra of the "as deposited" ice overlayers (solid line) on both the EG_2 and EG_6 SAMs are quite similar and agree with previous RA spectra of D_2O-ice overlayers deposited at low temperatures.[35,37] Also shown are the best-fit, simulated RA spectra (dotted lines) of Ia-ice. The main differences between the simulation and experiment for both SAMs appear above 2520 cm^{-1} (shaded areas in Figure 3a,b). Note that introduction of voids or mixing the Ia-ice with Ih-ice in different proportions cannot be used to improve the fit because voids/Ih-ice inclusion will shift the main peak toward low frequencies, i.e., in the wrong direction, cf. Figure 2b. Previous publications[33,50] suggest that the peaks above 2520 cm^{-1} in the D_2O-ice spectrum mainly belong to distorted vibrational modes that normally are referred to as surface ice modes.

The appearance of such modes is consistent with a "hit and stick" model where the D_2O molecules, because of the limited lateral mobility at 85 K, tend to attach at the position where they hit the SAM surface. This results in a defect-rich (coordination number less than four) D_2O-ice overlayer with a large amount of partially hydrogen bonded O−D groups and free oxygen orbital lobes exposed to the ice/vacuum interface. The sharp 2729 cm^{-1} peak, for example, is the free dangling O−D stretching mode.[35,50] Thus, it seems reasonable to assume that the "as deposited" ice layers are predominantly composed of a distorted and defect-rich amorphous-like ice structure with a large surface-to-volume ratio. As the sample temperature is increased, the D_2O molecules rearrange due to increased lateral mobility to form new bonds through interaction with neighboring D_2O molecules and/or the substrate surface. This leads to changes in internal structure and morphology of the ice overlayer. The general trend seen in the RA spectra recorded during annealing is that the main absorbance peak shifts to lower frequencies and increases in intensity (cf. Figure 2) at the same time as the sharp peak at 2729 cm^{-1} decreases in intensity. The change is fast and prominent for D_2O-ice overlayer on the EG_6 SAM, Figure 3b, whereas only small, but detectable, changes occur in the line shape for the D_2O-ice overlayer on the EG_2 SAM, Figure 3a. For example, the changes seen in Figure 3b after 2 min of annealing on the EG_6 SAM are essentially the same as those seen after 60 min in Figure 3a. Also shown in Figure 3a,b are the simulated RA spectra "best fits" (dotted lines). It is evident from Figure 3a,b that the fits to the experimental data improve for the annealed samples and that introduction of voids is necessary. As can be seen in Figure 3a, the structure of the D_2O-ice overlayer on the EG_2 SAM stays in an amorphous-like state during the first 20 min of annealing, and a small number of voids (10−20%) are necessary to obtain a good fit. After 20 min of annealing, the amount of amorphous ice decreases and it is necessary to introduce Ih-ice into the simulation while keeping the void fraction constant. Prolonged annealing increases the fraction of Ih-ice even further without influencing the void fraction. The final ice overlayer obtained after 60 min of annealing is according to our simulation composed of mixture of 70% Ia/30% Ih D_2O-ice with 20% voids.

The D_2O-ice overlayer on the EG_6 SAM displays a different behavior during annealing, Figure 3b. First of all, the transition from amorphous-like into crystalline-like ice (cf. Figure 2) is much faster than that on the EG_2 SAM. The transition occurs via a state that according to our simulations contains 50% Ia/50% Ih and 10% voids (2 min), into a fully developed state of 100% Ih-ice with 10% voids (5 min). After 5 min the only change occurring over time is an increase in the number of voids, up to 30% for 60 min at 140 K. Thus, the ice overlayer changes structure far more rapidly into a crystalline-like (Ih-ice) structure, with voids on the EG_6 SAM surface.

The properties of the two SAM substrates obviously influence the dynamics of the temperature-driven phase transition from amorphous- to crystalline-like D_2O-ice. The transition from a distorted amorphous-like phase on the EG_2 SAMs, consisting of all-trans ethylene glycol tails, is considerably slower than that on the EG_6 SAM with ethylene glycol tails in the helical conformation. This indicates, at a first glance, that the mobility, and thereby the ability to rearrange and form new and more stable ice structures, is higher on the EG_6 SAM surface. This is somewhat surprising since earlier publications suggest that the mobility of D_2O on a SAM substrate is critically dependent on the surface energy, and since EG_2 and EG_6 has the same surface energy, Θ_{H_2O} equals 27° and 28°,[51] respectively, one would expect the mobility to be more or less the same in both cases.[33,37,52] It is therefore clear that the surface energy is not the only parameter of the substrate that influences the phase behavior of the D_2O-ice overlayer. Another possibility is that the two SAM surfaces possess different types of sites that can act as nucleation sites for crystalline Ih-ice formation and

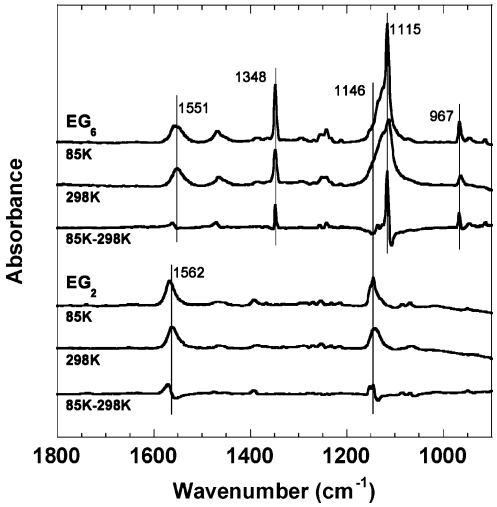

Figure 4. RA spectra recorded in the fingerprint region at different substrate temperatures for EG_2 and EG_6 SAMs. Upper panel: RA spectra recorded at 85 and 298 K, as well as the difference spectrum (85−298 K) for the EG_6 SAM. Lower panel: RA spectra at 85 and 298 K, as well as the difference spectrum (85−298 K) for the EG_2 SAM.

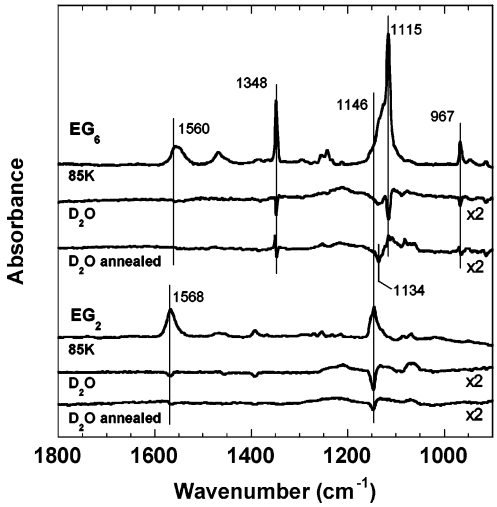

Figure 5. RA spectra in the fingerprint region recorded at 85 K before deposition of ∼2.5 ML of D_2O-ice. Also shown are the difference spectra obtained after subtraction of the 85 K spectrum from that obtained after D_2O deposition and after annealing of the sample at 140 K for 60 min, respectively. Upper panel: D_2O-ice on EG_6 SAM. Lower panel: D_2O-ice on EG_2 SAM.

growth. Wang et al.[32] showed recently in a theoretical work that the helical ethylene glycol conformation possesses a site that strongly interacts with water, and they suggested that this site could act as a potential nucleation site for crystalline ice growth. Thus, the existence of such a site may very well explain the rapid kinetics seen on the EG_6 SAM (see discussion below). We will in the following focus on the interactions between the ice overlayer and the EG_2 and EG_6 surfaces.

Properties of the SAM Surfaces. The outermost part of the molecules is of greatest interest when studying the ice−surface interactions, and these parts are OEG chains of varying length and conformation. The chemical structures of the EG_2 and EG_6 compounds shown in Scheme 1 reveal that they consist of a thiolated hydrocarbon backbone, connected via an amide link to the OEG chains. As the temperature of the thiol−SAM is altered, the structure of the monolayer generally changes due to the appearance of new intramolecular as well as intermolecular interactions.[51,53−56] These changes may result in different phases of the SAMs, and to the exposure of new parts of the SAMs to the ice overlayer. Wang et al.[32] showed, for example, in a theoretical study that all-trans and helical OEGs possess different types of binding sites for water. Moreover, Zolk et al.[31] used SFG to evaluate water penetration into the all-trans OEG portion of an EG_3 SAM, and they showed that a substantial penetration occurred all the way down to the alkyl barrier layer of the SAM (a SAM that is analogous to those formed by the molecules in Scheme 1). More recently Fick et al.[29] reported that the degree of water penetration depended on the OEG chain conformation, with high penetration into amorphous OEGs and low penetration into crystalline (helical) OEGs. We find these observations highly relevant although the reported experiments were performed under different experimental conditions (liquid water). The following sections will explore the structural transitions occurring in the OEG SAMs upon lowering the temperature as well as upon deposition of ice.

Temperature Dependence of the EG_2 and EG_6 SAM Structure. The room-temperature RA spectrum (298 K) of the EG_2 SAM, Figure 4 (lower portion), consists of two strong peaks in the fingerprint region, the amide II (C−N stretching + N−H bending) mode at 1562 cm^{-1} and the C−O−C stretching mode at 1146 cm^{-1}. The shape and position of the 1146 cm^{-1} peak is typical for OEG chains in the all-trans conformation. The RA spectrum of the EG_6 SAM (298 K), Figure 4 (upper portion), possesses the amide II peak at 1551 cm^{-1} and a few very sharp and intense peaks at 1348, 1115, and 967 cm^{-1}, respectively, that are attributed to C−O−C modes of the helical OEG chains.[19] Figure 4 shows also the low-temperature 85 K spectra of the two SAMs as well as the difference RA spectra 85−298 K.

The temperature dependence of the all-*trans*-OEG structure in the EG_2 SAM appears to be very small. The only changes that occur are the minute peak shifts and intensity changes appearing as derivative-like features in the difference spectrum. The temperature dependence is more pronounced in the EG_6 SAM spectra (upper portion), where the peaks characteristic for helical OEGs turn sharp and intense, and this effect is especially pronounced for the main peak at 1115 cm^{-1}. The shoulders on the high-frequency side of the main peak, which has been attributed to other conformational states of the EG_6 SAM (e.g., amorphous and all-trans),[19] appear with reduced relative intensities as compared to the main helical peak at 1115 cm^{-1}. Thus, the reduction of the motional broadening of the IR peaks clearly contributes to an overall intensity enhancement of the helical peaks for the EG_6 SAM, whereas subtle intensity changes are seen in the same region for the all-trans peaks in the EG_2 SAM. Returning back to 298 K after 85 K gives rise to RA spectra that are identical with those initially recorded at 298 K, i.e., no irreversible changes occur in the two SAM structures.

EG_n−D_2O Interaction. Approximately 6 Å (∼2 ML) of D_2O is being deposited onto the substrate surfaces at 85 K after which the structural changes due to the ice-SAM interactions are investigated with IRAS. The structure of D_2O deposited onto the two substrates is close to identical, compare the "as deposited" RA spectra in parts a and b of Figure 3. This is expected, since the EG_2 and EG_6 SAMs display essentially the same surface energy.[19] The corresponding RA spectra (in the fingerprint region) reveal the effects of D_2O-ice deposition on the supporting SAM structure, Figure 5. The lower panel of Figure 5 shows again the 85 K spectrum of the EG_2 SAM. Also shown are the difference spectra "D_2O" obtained after subtraction of the 85 K spectrum from that recorded after deposition of ∼6 Å of D_2O. Another difference spectrum "D_2O annealed"

obtained by subtracting the 85 K spectrum from that recorded after annealing the D_2O-ice overlayer at 140 K for 60 min and then returning back to 85 K is also shown.

The same set of RA spectra is shown for EG_6 SAM, Figure 5 (upper portion). The main effect seen in the EG_2 spectrum upon D_2O-ice deposition is the negative peak at 1146 cm^{-1}. Thus, deposition of ice appears to affect the all-trans structure of the EG_2 tail. A partial recovery of the all-trans structure (less negative peak at 1146 cm^{-1}) appears after annealing, but there is still a permanent perturbation of the SAM structure. A small, but detectable, decrease in intensity is also seen for the amide II peak at 1568 cm^{-1}. Taken together, our data for the EG_2 SAM suggest that the D_2O molecules penetrate into the outermost portion of the SAM and partly disturb the all-trans structure.

The effect on the EG_6 SAM upon D_2O deposition is mainly seen as a decrease in the intensity of the vibrational modes corresponding to the helical conformation of the OEG portion. The helical peaks at 1348, 1115, and 967 cm^{-1} appear as negative features, and this is also true for the peaks at 947 and 913 cm^{-1}, respectively. A negative peak is also seen at 1134 cm^{-1}, i.e., at a position that is characteristic for amorphous OEGs. Thus, deposition of D_2O on the EG_6 SAM appears to influence both the dominating helical conformation as well as the less abundant amorphous phase. The helical structure almost completely recovers after annealing at 140 K for 60 min, and the only helical features seen are the derivative-like peaks at 1348 and 967 cm^{-1}. Thus, very small permanent perturbations seem to occur in the helical structure of the EG_6 SAM. Nor do we observe any intensity changes in the amide II region. Thus, D_2O appears not to penetrate into the helical portion of the EG_6 SAM as in the case of the all-trans phase of the EG_2 SAM. The only prominent and permanent change seen in the RA spectrum obtained after annealing is the negative peak at about 1134 cm^{-1}. This might indicate that the amorphous chains, which are known to coexist with the helical chains in the EG_6 SAM[16] (see the discussion above about the shoulder on the high-frequency side of the main peak) offers a channel for D_2O penetration into the EG_6 assembly.

Our studies of the interactions between the SAM surface and the D_2O-ice overlayers clearly suggest that the D_2O penetration into and interaction with the helical and all-trans OEGs is different. The limited penetration into the EG_6 SAM is in agreement with recent work by Fick et al.,[29] who reported on a very small penetration of water into crystalline, helical, OEGs. The rapid and pronounced transition from amorphous-like to crystalline-like D_2O-ice on the EG_6 SAM upon isothermal annealing, Figure 3b, is also consistent with presence of specific nucleation sites in the helical structure as suggested by Wang et al.[32] These sites are localized within the very outermost portion of the helical chain (i.e., near the ice/OEG interface). The significant penetration into and interaction with the all-trans chain may thus explain why the phase transition above is much slower upon isothermal annealing of D_2O-ice on the EG_2 SAM than on the EG_6 SAM, cf. the evolution of the peaks characteristic of crystalline-like ice in Figure 3a,b.

This combined theoretical and experimental temperature programmed IRAS approach reveals that changes in molecular conformation within the outermost portion of SAMs dramatically influence the interaction with ultrathin D_2O-ice overlayers. We show, for example, that the kinetics of the amorphous to crystalline phase transition is strongly influenced by D_2O penetration and interaction with sites within the OEG portions. The kinetics is fast on the helical EG_6 SAM (nonpenetrating) and slow on the all-trans EG_2 SAM (penetrating). Moreover, our theoretical work reveals the importance of introducing ice mixtures and voids in the optical model of the ice overlayer in order to be able to accurately simulate RA spectra of the ultrathin D_2O-ice overlayer. The introduction of voids is particularly important for the simulation of RA spectra of D_2O-ice overlayers with a large hexagonal Ih-ice content.

Conclusions

In the first part of this study we show through comparison of experimental and simulated IR reflection spectra that temperature-treated ultrathin ice overlayers on hydroxyl and oligo(ethylene glycol)-terminated SAMs can be interpreted in terms of structures of the Ih-ice phase with considerable void content. The simulations clearly show that it is necessary to include voids to be able to describe the phase transitions occurring in such D_2O-ice overlayers. The agreement between experimental and simulated spectra is extremely good for crystalline-like, Ih-ice. The fits are not as good for ultrathin amorphous-like D_2O-ice because it consists of a large number of defects, e.g., free dangling O−D bonds, which in the RA spectrum show up as so-called surface modes. These modes are not taken into account in the modeling of the effective dielectric function of the D_2O-ice.

The second part of the study is devoted to studies of water-induced perturbations of the molecular conformation in the OEG portion of the SAMs. Our data show that D_2O penetrates, binds, and permanently disturbs the all-trans and amorphous portions of the EG_2 and EG_6 SAMs, respectively, whereas no such effects can be observed for the helical chains of the EG_6 SAM. The significant interaction with the all-trans chains is believed to be the main cause for the slow kinetics observed for the amorphous-like to crystalline-like phase transitions of D_2O-ice on the EG_2 SAM surface.

These types of fundamental observations contribute to an improved understanding of the temperature-dependent behavior of interfacial water on organic surfaces, an important area in biology, and point out the value of using vibrational spectroscopy coupled with spectral simulations to analyze complex water/ice structures on organic surfaces.

Acknowledgment. This work was supported by the Swedish research Council (VR), the Swedish Foundation for Strategic Research (SSF) through the Biomimetic Materials Science program (B.L. and MÖ) and the U.S. National Science Foundation (D.L.A. and M.G.).

Supporting Information Available: Details of the comparison of Maxwell Garnett and Bruggeman effective medium approzimation applied to ultrathin D_2O-ice. This material is available free of charge via the Internet at http://pubs.acs.org.

References and Notes

(1) Nuzzo, R. G.; Allara, D. L. *J. Am. Chem. Soc.* **1983**, *105*, 4481.
(2) Riepl, M.; Enander, K.; Liedberg, B.; Schaferling, M.; Kruschina, M.; Ortigao, F. *Langmuir* **2002**, *18*, 7016.
(3) Svedhem, S.; Ohberg, L.; Borrelli, S.; Valiokas, R.; Andersson, M.; Oscarson, S.; Svensson, S. C. T.; Liedberg, B.; Konradsson, P. *Langmuir* **2002**, *18*, 2848.
(4) Lahiri, J.; Kalal, P.; Frutos, A. G.; Jonas, S. T.; Schaeffler, R. *Langmuir* **2000**, *16*, 7805.
(5) Mirkin, C. A. *Inorg. Chem.* **2000**, *39*, 2258.
(6) Demers, L. M.; Mirkin, C. A.; Mucic, R. C.; Reynolds, R. A.; Letsinger, R. L.; Elghanian, R.; Viswanadham, G. *Anal. Chem.* **2000**, *72*, 5535.
(7) Lindholm-Sethson, B. *Langmuir* **1996**, *12*, 3305.

(8) Radford, P. T.; French, M.; Creager, S. E. *Anal. Chem.* **1999**, *71*, 5101.
(9) Sumner, J. J.; Weber, K. S.; Hockett, L. A.; Creager, S. E. *J. Phys. Chem. B* **2000**, *104*, 7449.
(10) Tian, Y.; Mao, L. Q.; Okajima, T.; Ohsaka, T. *Anal. Chem.* **2004**, *76*, 4162.
(11) Lee, S.; Puck, A.; Graupe, M.; Colorado, R.; Shon, Y. S.; Lee, T. R.; Perry, S. S. *Langmuir* **2001**, *17*, 7364.
(12) Xiao, X. D.; Hu, J.; Charych, D. H.; Salmeron, M. *Langmuir* **1996**, *12*, 235.
(13) Jenkins, A. T. A.; Bushby, R. J.; Evans, S. D.; Knoll, W.; Offenhausser, A.; Ogier, S. D. *Langmuir* **2002**, *18*, 3176.
(14) Heyse, S.; Ernst, O. P.; Dienes, Z.; Hofmann, K. P.; Vogel, H. *Biochemistry* **1998**, *37*, 507.
(15) Valiokas, R.; Ostblom, M.; Svedhem, S.; Svensson, S. C. T.; Liedberg, B. *J. Phys. Chem.* B **2000**, *104*, 7565.
(16) Qian, X. P.; Metallo, S. J.; Choi, I. S.; Wu, H. K.; Liang, M. N.; Whitesides, G. M. *Anal. Chem.* **2002**, *74*, 1805.
(17) Kane, R. S.; Deschatelets, P.; Whitesides, G. M. *Langmuir* **2003**, *19*, 2388.
(18) Chapman, R. G.; Ostuni, E.; Yan, L.; Whitesides, G. M. *Langmuir* **2000**, *16*, 6927.
(19) Valiokas, R.; Svedhem, S.; Svensson, S. C. T.; Liedberg, B. *Langmuir* **1999**, *15*, 3390.
(20) Pale-Grosdemange, C.; Simon, E. S.; Prime, K. L.; Whitesides, G. M. *J. Am. Chem. Soc.* **1991**, *113*, 12.
(21) Schwendel, D.; Dahint, R.; Herrwerth, S.; Schloerholz, M.; Eck, W.; Grunze, M. *Langmuir* **2001**, *17*, 5717.
(22) Vanderah, D. J.; Valincius, G.; Meuse, C. W. *Langmuir* **2002**, *18*, 4674.
(23) Harder, P.; Grunze, M.; Dahint, R.; Whitesides, G. M.; Laibinis, P. E. *J. Phys. Chem. B* **1998**, *102*, 426.
(24) Benesch, J.; Svedhem, S.; Svensson, S. C. T.; Valiokas, R.; Liedberg, B.; Tengvall, P. *J. Biomater. Sci., Polym. Ed.* **2001**, *12*, 581.
(25) Vogler, E. A. *J. Biomater. Sci., Polym. Ed.* **1999**, *10*, 1015.
(26) Kasemo, B. *Surf. Sci.* **2002**, *500*, 656.
(27) Israelachvili, J.; Wennerström, H. *Nature* **1996**, *379*, 219.
(28) Pertsin, A. J.; Hayashi, T.; Grunze, M. *J. Phys. Chem. B* **2002**, *106*, 12274.
(29) Fick, J.; Steitz, R.; Leiner, V.; Tokumitsu, S.; Himmelhaus, M.; Grunze, M. *Langmuir* **2004**, *20*, 3848.
(30) Pertsin, A. J.; Grunze, M. *Langmuir* **2000**, *16*, 8829.
(31) Zolk, M.; Eisert, F.; Pipper, J.; Herrwerth, S.; Eck, W.; Buck, M.; Grunze, M. *Langmuir* **2000**, *16*, 5849.
(32) Wang, R. L. C.; Kreuzer, H. J.; Grunze, M. *J. Phys. Chem. B* **1997**, *101*, 9767.
(33) Engquist, I. *Microscopic wetting*: *structural and morphological studies of thin ice on self-assembled monolayers*. Thesis, Linköping University, 1996.
(34) Engquist, I.; Lestelius, M.; Liedberg, B. *Langmuir* **1997**, *13*, 4003.
(35) Engquist, I.; Liedberg, B. *J. Phys. Chem.* **1996**, *100*, 20089.
(36) Engquist, I.; Lundstrom, I.; Liedberg, B. *J. Phys. Chem.* **1995**, *99*, 12257.
(37) Engquist, I.; Lundstrom, I.; Liedberg, B.; Parikh, A. N.; Allara, D. L. *J. Chem. Phys.* **1997**, *106*, 3038.
(38) Svedhem, S.; Hollander, C. A.; Shi, J.; Konradsson, P.; Liedberg, B.; Svensson, S. C. T. *J. Org. Chem.* **2001**, *66*, 4494.
(39) Yeh, P. *Optical waves in layered media*; Wiley: New York, 1988.
(40) Parikh, A. N.; Allara, D. L. *J. Chem. Phys.* **1992**, *96*, 927.
(41) Palik, E. D. *Handbook of optical constants of solids*; Academic Press: Orlando, FL, 1998.
(42) Bergren, M. S.; Schuh, D.; Sceats, M. G.; Rice, S. A. *J. Chem. Phys.* **1978**, *69*, 3477.
(43) Maxwell Garnett, J. C. *Philos. Trans. R. Soc. London, Ser. A* **1904**, *203*, 285.
(44) Maxwell Garnett, J. C. *Philos. Trans. R. Soc. London, Ser. A* **1906**, *205*, 237.
(45) Tao, Y. T.; Lin, W. L.; Hietpas, G. D.; Allara, D. L. *J. Phys. Chem. B* **1997**, *101*, 9732.
(46) Tao, Y. T.; Hietpas, G. D.; Allara, D. L. *J. Am. Chem. Soc.* **1996**, *118*, 6724.
(47) Aspnes, D. E. *Thin Solid Films* **1982**, *89*, 249.
(48) Foss, C. A.; Hornyak, G. L.; Stockert, J. A.; Martin, C. R. *J. Phys. Chem.* **1992**, *96*, 7497.
(49) Gehr, R. J.; Boyd, R. W. *Chem. Mater.* **1996**, *8*, 1807.
(50) Rowland, B.; Kadagathur, N. S.; Devlin, J. P.; Buch, V.; Feldman, T.; Wojcik, M. J. *J. Chem. Phys.* **1995**, *102*, 8328.
(51) Valiokas, R.; Svedhem, S.; Ostblom, M.; Svensson, S. C. T.; Liedberg, B. *J. Phys. Chem. B* **2001**, *105*, 5459.
(52) Nuzzo, R. G.; Zegarski, B. P.; Korenic, E. M.; Dubois, L. H. *J. Phys. Chem.* **1992**, *96*, 1355.
(53) Nuzzo, R. G.; Korenic, E. M.; Dubois, L. H. *J. Chem. Phys* **1990**, *93*, 767.
(54) Garand, E.; Picard, J. F.; Rowntree, P. *J. Phys. Chem. B* **2004**, *108*, 8182.
(55) Bensebaa, F.; Ellis, T. H.; Badia, A.; Lennox, R. B. *J. Vac. Sci. Technol., A* **1995**, *13*, 1331.
(56) Valiokas, R.; Ostblom, M.; Svedhem, S.; Svensson, S. C. T.; Liedberg, B. *J. Phys. Chem.* B **2002**, *106*, 10401.